42nd ERF, September 5–8, 2016, Lille, FR
50

EXPERIMENTS ON THE HELICOPTER-OBSTACLE AERODYNAMIC INTERFERENCE IN ABSENCE OF EXTERNAL WIND

D. Zagaglia[*,#], G. Gibertini[*], M. Giuni[†], R.B. Green[†]

[*]: Politecnico di Milano - Dipartimento di Scienze e Tecnologie Aerospaziali
Campus Bovisa, Via La Masa 34, 20156 Milano, Italy
[†]: University of Glasgow - Aerospace Sciences Division, School of Engineering
James Watt Building South, Glasgow G12 8QQ, UK

[#] e–mail: daniele.zagaglia@polimi.it

Keywords: Rotorcraft, Aerodynamics, Vortex Interaction, Particle Image Velocimetry (PIV), Ground Obstacle.

Abstract

The rotor-obstacle interaction has become a challenging research topic in the last few years. In the present paper a comprehensive experimental survey carried out at University of Glasgow is described, taking advantage of two different rotor rigs and several experimental techniques. The results are then compared with those already obtained for a similar investigation at Politecnico di Milano. The experimental database comprises load measurements on the rotor (in order to assess the rotor performance for different positions with respect to a cubic obstacle), Laser Doppler Anemometry (LDA) measurements of the rotor inflow and Stereoscopic Particle Image Velocimetry (SPIV) measurements in the region between the rotor and the obstacle. Despite a few slight differences in geometry and test conditions, the two databases show several similarities that are analysed in the paper.

Nomenclature

A	Rotor disc area
c	Blade chord
c_T	Thrust Coefficient, $T/\left(\rho V_{\text{TIP}}^2 A\right)$
c_Q	Torque Coefficient, $Q/\left(\rho V_{\text{TIP}}^2 AR\right)$
c_{Mx}	$x-$Moment Coeff., $M_x/\left(\rho V_{\text{TIP}}^2 AR\right)$
c_{My}	$y-$Moment Coeff,, $M_y/\left(\rho V_{\text{TIP}}^2 AR\right)$
$CIRA$	Italian Aerospace Centre
D	Rotor disc diameter
DLR	German Aerospace Centre
FM	Figure of Merit, $c_T^{3/2}/(\sqrt{2}c_Q)$
IGE	In Ground Effect condition
L	Cubic obstacle size
LDA	Laser Doppler Anemometry
M	PIV optical magnification factor
N_b	Number of blades
NLR	Dutch Aerospace Centre
OGE	Out of Ground Effect condition
$ONERA$	French Aerospace Centre
POLIMI	Politecnico di Milano
PIV	Particle Image Velocimetry
R	Rotor disc radius
SPIV	Stereoscopic Particle Image Velocimetry
UoG	University of Glasgow
v	Out-of-plane velocity component
(X, Y, Z)	Absolute reference system
(x, y, z)	Rotor reference system
Δt	Time delay between two laser pulses
ϵ_u	Uncertainty on the in-plane velocity components
$\epsilon_{u,\text{op}}$	Uncertainty on the out-of-plane velocity component

ρ	Air density
σ	Rotor Solidity, defined as $N_b c/(\pi R)$
θ	Camera separation semi-angle
θ_c	Collective Pitch angle
Ω	Rotor rotational frequency

1 INTRODUCTION

Helicopters, due to their capability of managing hovering flight, are highly exploited in missions within confined areas. The aerodynamic interaction between the rotor-induced wake and the surrounding obstacles generates, on the one hand, high compensatory workload for the pilot and degradation of aircraft performance, on the other hand unsteady forces which can stress the structure of the obstacle. A few experimental and numerical investigations have been produced on this topic in the last few years, especially for the Dynamic Interface problem [1], where the helicopter interacts with the superstructures which are usually present on ship decks (see for instance [2] and [3]). For what concerns the experimental literature on this topic, a few geometries and configurations were analysed by means of different experimental techniques, such as loads measurements of the helicopter [4], velocity measurements in the rotor inflow region and wake [5] and Particle Image Velocimetry [6]. A comprehensive analysis of the performance of a fully-articulated rotor between two vertical walls was achieved by [7].

Despite the presence of a fair number of numerical and experimental works, a systematic study of these aerodynamic phenomena is lacking. The GARTEUR Action Group 22 *"Forces on Obstacles in Rotor Wake"*, comprising several universities (Politecnico di Milano, University of Glasgow, University of Liverpool, National Technical university of Athens) and research institutes (CIRA, DLR, ONERA, NLR), originates from the idea of promoting activities which could contribute to a better understanding of these phenomena. An extended database of a model rotor hovering next to a cubic obstacle, comprising several measurement points and experimental techniques, was produced at University of Glasgow with a thorough insight on the interacting flow, which is the subject of the present paper. In the same framework, the production of an experimental database had already been carried out at Politecnico di Milano [8], analysing the case of a model helicopter with fuselage interacting with a cuboid obstacle, in absence of wind.

The purpose of the present work is to describe the extended experimental database produced in Glasgow for the rotor-obstacle aerodynamic investigation,using a simplified geometry (cubic obstacle) and different kinds of experimental surveys, i.e. load measurements on the rotor, Laser Doppler Anemometry (LDA) in the rotor inflow region and Stereoscopic Particle Image Velocimetry (SPIV) of the the flowfield. The results show several similarities with respect to what had already been done at Politecnico di Milano, and these similarities will be the subject of further analysis in this paper.

2 THE EXPERIMENTAL APPARATUS

2.1 Glasgow Test rig description and Test matrix

Two different rotor rigs were employed at university of Glasgow, whose main features are reported in Table 1 (Large and "wee" rotor rig), together with those of the Politecnico di Milano Test Rig. The experimental campaign consisted of a set of tests reproducing hovering flight conditions at different positions with respect to a simplified obstacle with a cubic shape (the measurement points are represented in Figure 2). The measurements were carried out in the symmetry plane of the problem ($Y/R = 0$).

The data that will be presented in this paper follow the conventions of Figure 2 and Figure 3. Two different reference systems are defined: the global reference system (X, Y, Z) which defines the position of the rotor hub centre with respect to the obstacle and the rotor reference system (x, y, z), which corresponds to the load-cell axes. The origin of the absolute (X, Y, Z) coordinate system is fixed and it is placed on the floor, at the obstacle mid-span (as in Figure 3).

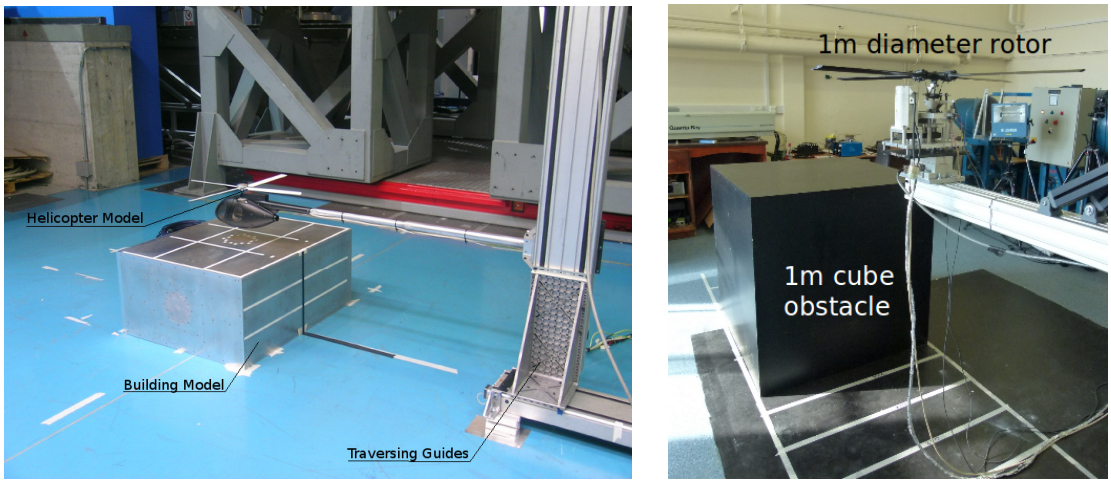

(a) Polimi experimental test rig

(b) Glasgow Large rotor rig

(c) Glasgow "Wee" rotor rig

Figure 1: Pictures of the considered Rotor Rig

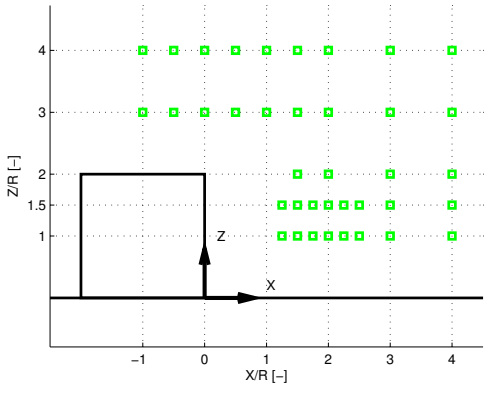

Figure 2: Measurement points in the problem symmetry plane ($Y/R = 0$). Each red circle represents the position of the rotor hub-centre for the corresponding measurement.

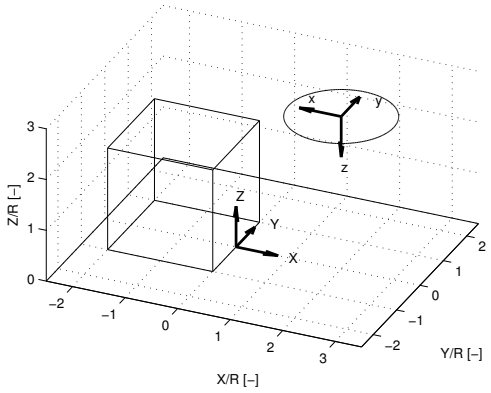

Figure 3: Absolute and Rotor reference systems.

The Large rotor rig (Figure 1b) was instrumented with a 6-components load cell, so that the forces and the moments on the rotor could be monitored. LDA measurements of the rotor inflow were performed in order to understand how the interacting flow field affected the rotor performance. Eventually a Stereo-PIV campaign was carried out on the "Wee" rotor rig (Figure 1c) in order to disclose the main features of the interacting flow field in a few relevant configurations.

As previously stated, the Large rotor rig was instrumented with a 6-components load cell which allowed the measurements of the forces and moments generated by the rotor. The employed load cell was an AMTI MC36, whose amplifier was set at a very high gain so that it would respond to the forces and moments. The nominal accuracy of the load cell was 0.25% of the full-scale output, corresponding approximately to 0.5% of the measured thrust in Out of Ground Effect condition.

The rotor inflow measurements were carried out by means of a Dantec 2D FiberFlow two-component Laser Doppler Anemometry (LDA) system along the rotor x and y axes (see the Reference system of Figure 3), 4 cm ($4\%D$) above the rotor plane. 7500 valid samples were taken at every measurement point, with accuracy of approximately 0.02 m/s corresponding to 0.4% of the maximum inflow velocity. The LDA system was mounted on a 3D traverse system allowing positioning with accuracy of less than 0.1 mm.

The Stereoscopic PIV was used to investigate the flow in the region between the obstacle and the rotor of the "Wee" rotor rig. These measurements were carried out by means of a LaVision system running Davis 8. The images were acquired by two Phantom v341 cameras, whose resolution was 4Mpixel. The seeded flow was illuminated by a Nd:YAG laser capable of 100mJ pulses at a maximum repetition rate of 200Hz, thus allowing time resolved measurement of the flow field development to be made. However only the ensemble-averaged measurements over 500 image pairs are addressed in the present paper.

The image pairs were post-processed by means of the Davis 8 software using 32×32 pixels interrogation windows with an overlap factor of 50%. The uncertainty of the velocity measurement was estimated (according to [9]) to be $\epsilon_u = \frac{1}{\sqrt{2}} \frac{0.1}{M\Delta t} = 0.1\ m/s$ for the in-plane velocity components and $\epsilon_{u,\mathrm{op}} = \frac{1}{\sqrt{2}\tan\theta} \frac{0.1}{M\Delta t} = 0.33\ m/s$ for the out-of-plane component, assuming a maximum displacement error of 0.1 pixels since a gaussian sub-pixel interpolation algorithm was used. An optical magnification factor of M =3.4161 pixel/m was used, together with a pulse separation time of $\Delta t = 200\ \mu s$ and $\theta = 15°$, corresponding to half of the camera separation angle.

2.2 Politecnico di Milano Test rig description and Test matrix

The experimental rig designed at Politecnico di Milano (Figure 1a), who has already been presented at the 40^{th} ERF [10], essentially consisted of a helicopter model and a geometric obstacle that ideally represented a building. The rotor had four untwisted rectangular blades and a diameter of 0.75 m. No swash plate was included in the present set up, thus the blades pitch angle was fixed to 10°. A six-components balance embedded inside the fuselage was used to measure the forces and moments acting on the rotor. The building model, made available by courtesy of DLR, was a cuboid box (0.45 m × 0.8 m × 1 m) with several pressure taps. The experimental campaign consisted of a set of tests reproducing hovering flight conditions at different positions with respect to the obstacle. The measurement of the loads acting on the rotor and of the pressure distributions over the obstacle external surfaces enabled to achieve information about the effects of this aerodynamic interaction both on the helicopter and on the building models. Moreover, Particle Image Velocimetry (PIV) was used to investigate the details of the interacting flow field in some interesting conditions. For further details of the Polimi setup, please refer to [8].

Characteristics	POLIMI	Glasgow Large rig	Glasgow "Wee" rig
Obstacle size	1m × 0.8m × 0.45m	1m × 1m × 1m	0.3m × 0.3m × 0.3m
Fuselage	Present	Not Present	Not Present
Rotor Diameter	0.75 m	1 m	0.3 m
Number of blades	4	4	2
Blade chord	32 mm	53 mm	31.7 mm
Solidity	0.11	0.135	0.134
Collective pitch	10°	8°	8°
Rotor Rotational frequency	2480 RPM (41.3 Hz)	1200 RPM (20 Hz)	4000 RPM (66.6 Hz)
Reynolds Num. at blade tip	212000	220000	132000
Mach Num. at blade tip	0.29	0.18	0.18
Type of Experiment	Loads meas. Pressure meas. 2D-PIV	Loads meas. LDA	Stereo-PIV Pressure meas.

Table 1: Main features of the Rotor Rigs

3 RESULTS FOR THE UNIVERSITY OF GLASGOW EXPERIMENTAL CAMPAIGN

In this section we analyse the main results of the experimental survey. The load measurements for the different rotor position are presented in Fig. 4 (plots) and Fig. 5, the LDA inflow measurements along the x and y axes are presented in Fig. 6 and finally the PIV measurements are presented in Fig. 7 (in-plane velocity magnitude contours and streamlines).

A set of load measurements were initially carried out in order to qualify the rotor performance in absence of the obstacle. The rotor was placed as high as possible ($Z/R = 4$) in order to assess the Out-of-Ground-Effect (OGE) condition. A $c_{T,\mathrm{OGE}}$ of $7.36 \cdot 10^{-3}$ and a $c_{Q,\mathrm{OGE}}$ of $8.75 \cdot 10^{-4}$ were obtained, leading to a Figure of Merit of FM_{OGE}=0.51.

Variation of the thrust coefficient with respect to the out-of-ground-effect (OGE) condition is presented in the plots of Figure 4a and 5a. The typical thrust increase (up to 20%) due to the ground effect can be appreciated in both the region over the centre of the obstacle and far from the obstacle, since the relative distance to the closest surface (either the floor or the top of the obstacle) is the same ($1R$) and the rotor projection lies completely on the obstacle top face. However two main regions where the rotor performance deviates from the nominal behaviour can be observed.

The first region is the one above the edge of the obstacle, where the thrust coefficient decreases as the rotor is positioned outwards, owing to the minority of the rotor lying over the upper surface of the obstacle (as already observed in [8]). This phenomenon can be appreciated also in the inflow profile of Figure 6a measured by means of the LDA system. In this case a gradual reduction of the inflow velocity is observed going from $X/R = 1$ to $X/R = -1$, as prescribed by the ground effect. However, one would expect this variation to be non-symmetrical, since only part of the rotor projection lies on the top of the obstacle and thus is affected by the ground effect. Conversely this appears not to be the case since the inflow profile of Fig. 6a is pretty symmetrical. This is also testified by the fact that the the pitch and roll moments of Fig. 4c and 4d are quite close to zero in the region $-1 < X/R < 1$. An additional interesting moment behaviour can be observed moving the rotor away from the obstacle ($1 < X/R < 3$) at the same heights ($Z/R = 3, 4$), where a positive $y-$ moment develops on the rotor, which fades out in the outer region ($X/R > 4$).

The second region, probably of more interest, is the one just beside the obstacle ($1 < X/R < 3$, $1 < Z/R < 3$), where a severe ground effect reduction can be observed, since the thrust coefficient drops to a value slightly

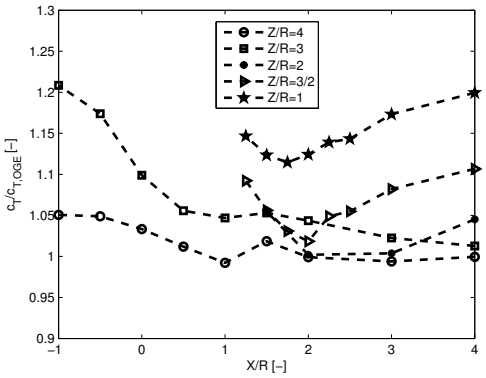

(a) Ratio between the Thrust Coefficient c_T and the one measured in OGE

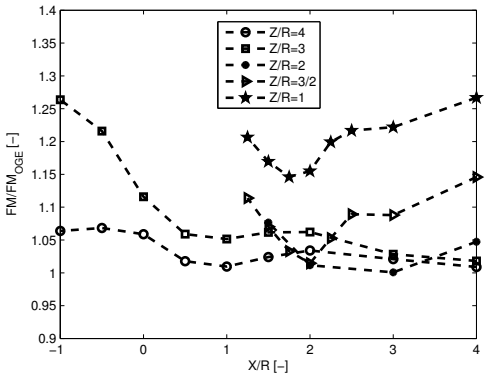

(b) Ratio between the Figure of Merit FM and the one measured in OGE

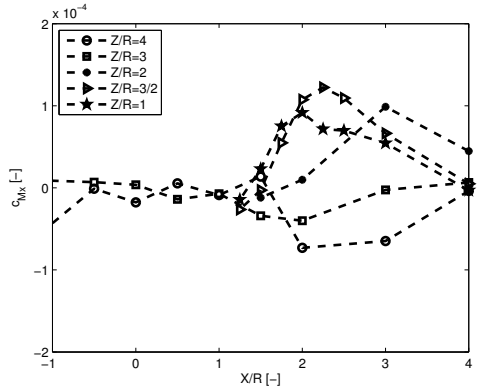

(c) x-moment coefficient

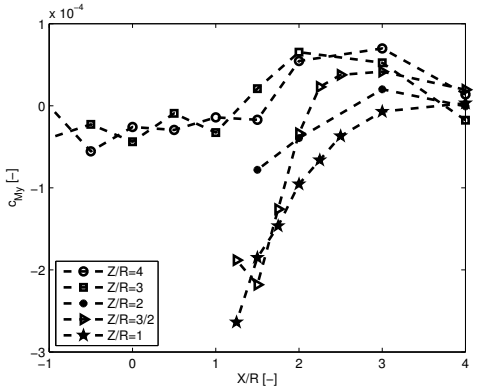

(d) y-moment coefficient

Figure 4: Loads acting on the rotor vs rotor position

below the OGE one, even at low heights. This behaviour is caused by the development of a recirculation region caused by the fact that the rotor wake, once deflected by the ground, is deflected again by the obstacle and then re-ingested by the rotor itself. This recirculation region, which is evident in the PIV flow-fields of Figure 7, causes an increased induced velocity and a consequent loss of thrust, similar to a partial vortex ring state. This effect is deeply dependent on both the rotor height and distance from the obstacle. A maximum thrust loss of 8% with respect to the furthest rotor position at the same height can be observed at $Z/R = 1, 3/2$, whereas at $Z/R = 2$ the maximum thrust loss is lower (approximately 4 %). Moreover one can appreciate the fact that the thrust loss is not monotonic when getting closer to the obstacle, but it presents a local minimum at approximately $X/R = 2$. This can be explained looking at Fig. 7, where at $X/R = 2$ (Fig.7d, 7e, 7f) the in-plane velocity on the edge of the obstacle (the green layer) is higher than in the other cases (approximately 4 m/s instead of 2.5), thus implying a stronger recirculation. In the other cases (further and closer to the obstacle) most of the air probably flows on the side of the obstacle instead of being redirected upwards. The effect of the obstacle start to be negligible when the rotor is further than 4 radia from the obstacle itself.

Another important feature of this region is the arising of strong pitching and rolling moments (up to 30% of the measured torque). This is due to the fact that the previously-introduced recirculation region mainly affects the portion of the rotor closer to the obstacle as it is shown in Figure 6c, where an increased

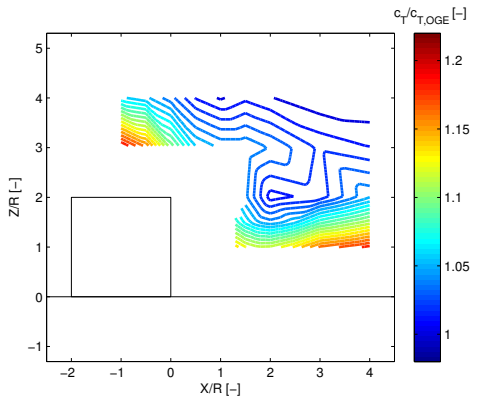

(a) Ratio between the Thrust Coefficient c_T and the one measured in OGE

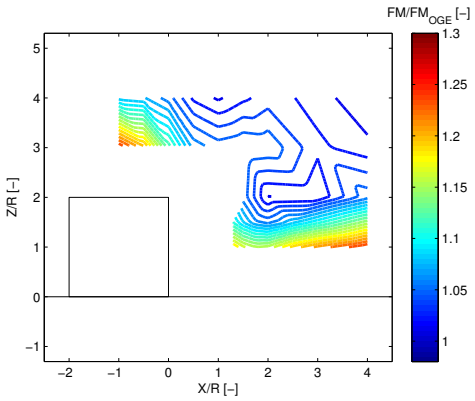

(b) Ratio between the Figure of Merit FM and the one measured in OGE

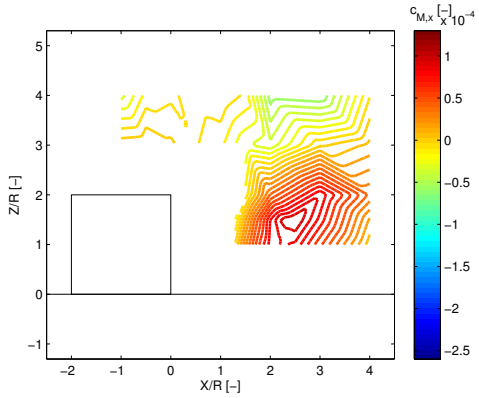

(c) x-moment coefficient

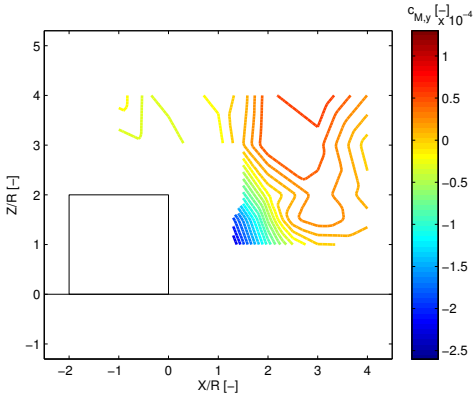

(d) y-moment coefficient

Figure 5: Contours of the Loads acting on the rotor vs rotor position

induced velocity can be observed in the left portion of the inflow profile for $X/R = 3/2$. Consequently, a negative c_{My} moment is generated on the rotor, which is evident in Figure 4d and 5d for $Z/R = 3/2$ and $Z/R = 2$ close to the obstacle, which is equivalent to a pitching nose-down moment if a helicopter was facing the wall. It must be pointed out that, since we are dealing with a fixed rotor without flap and lag hinges, the blade dynamics is more similar to the one of a propeller than to the one of an fully-articulated rotor, implying that the the rotor responds without the typical 90 degrees lag. However a little lag is nevertheless present due to the blade flexibility, thus probably explaining the contextual presence in this region of a $x-$ moment in the plots of Figure 4c and 5c (even if with a much smaller value with respect to the $y-$moment).

For what concerns the torque measurements, very limited variations were observed among all the rotor positions (less than 2%), leading to a Figure of Merit behaviour (Figures 4b and 5b) that is very similar to the thrust coefficient one.

The in-plane velocity contours and streamlines are presented in Figure 7, in order to disclose the main features of the flow-field. As we can appreciate, the already introduced recirculation region is present in all the cases, even though its morphology is highly case-dependant. At $X/R = 3/2$ (Figures 7a, 7b, 7c) we can appreciate that the rotor slipstream does not impinge on the floor before being deflected towards the obstacle, but impinges directly on the obstacle. This is due to the formation of a counter-rotating (with respect to the main one) recirculation region on the floor.

This region is pushed towards the obstacle as the rotor is moved downwards. At $X/R = 2$ (Figures 7d, 7e, 7f), as already highlighted in the previous paragraphs, the rotor wake impinges on the floor before being deflected by the obstacle and re-ingested by the rotor. The air-layer that goes upwards close to the obstacle is thicker and faster than the other cases, probably indicating a stronger interaction with the rotor (confirmed, as previously stated, by the thrust measurements). Eventually at $X/R = 3$ (Figures 7g, 7h, 7i) the flow pattern is very similar to a non-disturbed rotor wake in ground effect, suggesting that the interaction in this case is weaker (as the load measurements confirm).

4 COMPARISON WITH THE POLIMI DATABASE

As previously stated, even though the UoG and POLIMI setup and testing conditions were different, several similarities can be found in the results of the two experimental campaigns.

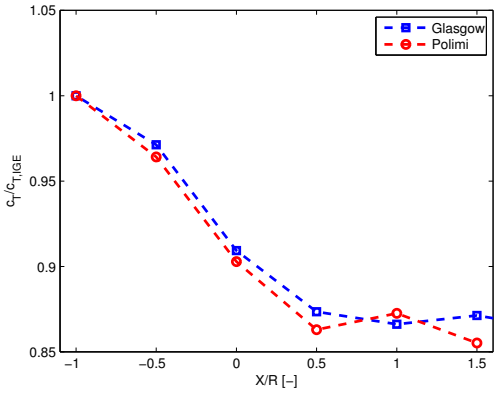

Figure 8: Thrust coefficient as function of the rotor distance from the obstacle edge during an horizontal sweep over the obstacle. Comparison between POLIMI and UoG database

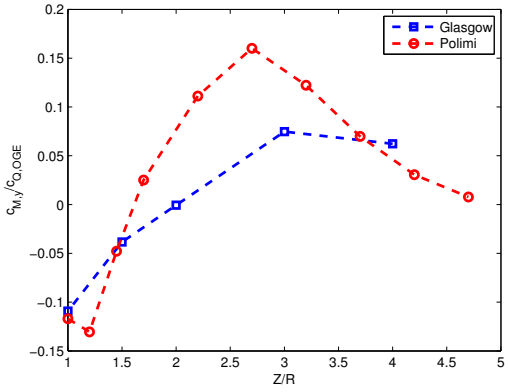

Figure 9: $y-$moment coefficient as function of the rotor height during a vertical sweep beside the obstacle, at $X/R = 2$. Comparison between POLIMI and UoG database

Let us start considering the case of a sweep in the X direction over the edge of the obstacle. This corresponds to an horizontal sweep at $Z/R = 3/2$ for the UoG database, and to the same sweep at $Z/R = 2$ for the POLIMI database (Test 5 of Ref.[8]). Figure 8 presents the variation of the thrust coefficient for both databases in this configuration. $X/R = -1$ corresponds to the rotor being fully over the obstacle, $X/R = 0$ to the rotor centre being over the edge of the obstacle and so on, moving the rotor away from the obstacle for increasing X/R. The results are presented in terms of the ratio with respect to the condition where the rotor is fully in ground effect condition on the obstacle, i.e. $X/R = -1$). As we can appreciate, the two experiments highlight the same performance trend which is probably due to the fact that the ground effect experienced by the rotor is proportional to the percentage of the rotor projection lying on the top of the obstacle, which is the same, at each location, for the two setups. Moreover during this $X-$sweep, very low pitch and roll (close to zero) moments were observed in the Polimi Database, exactly as in the UoG one. As previously stated in section 3, this can be considered a peculiar behaviour, since only part of the rotor projection lies on the top of the obstacle and thus one would expect a non-symmetrical disk loading and a consequent moment. Nevertheless this behaviour was observed in both experiments, thus confirming the effective occurrence of this

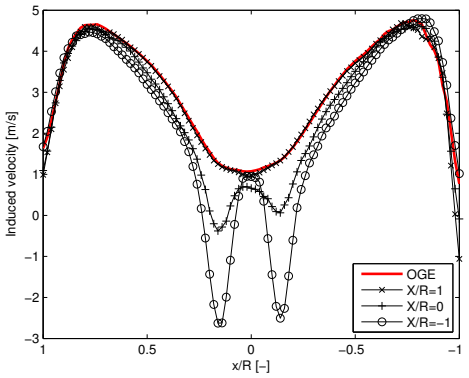

(a) $Z/R = 3$, Sweep in the x direction

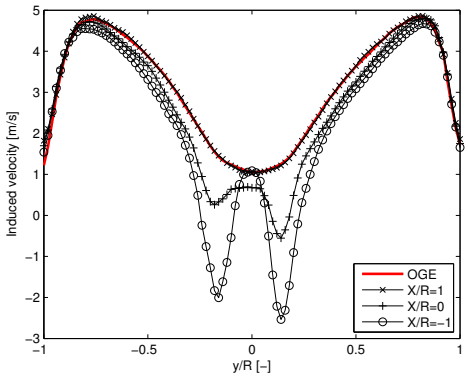

(b) $Z/R = 3$, Sweep in the y direction

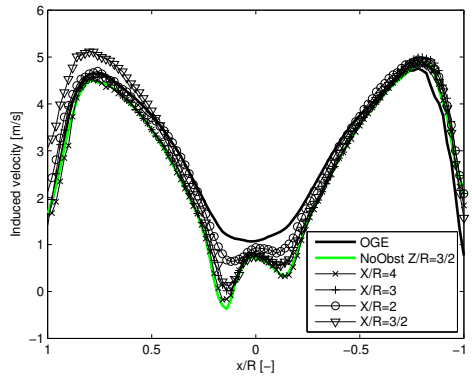

(c) $Z/R = 3/2$, Sweep in the x direction

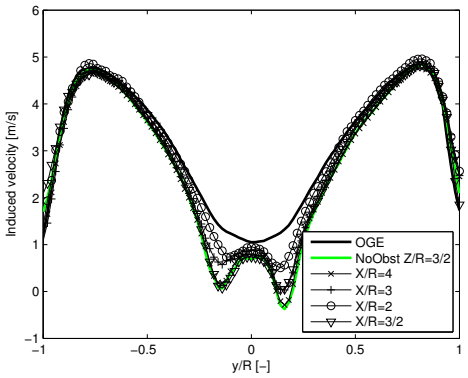

(d) $Z/R = 3/2$, Sweep in the y direction

Figure 6: Induced velocity 4 cm above the rotor in the x (at $y/R = 0$) and y (at $x/R = 0$) directions. According to the convention of Fig 3, a positive induced velocity points downwards. The obstacle is on the left of the plots

phenomenon.

Let us now consider the case of a vertical sweep in the Z direction on the side of the obstacle at $X/R = 2$, corresponding to Test 4 of Ref.[8]. As previously recalled in section 3, the region just beside the building is characterised by a recirculation region that causes a loss of thrust and a conspicuous pitch moment on the rotor due to the increased induced velocity on just the part of the rotor which faces the obstacle. Fig. 9 presents the comparison between the $y-$moment coefficient (divided by the OGE torque) of the two experiments for the vertical sweep. As it can be appreciated, both experiments show the exact same behaviour, even if with different moment values that probably depend on the slight differences in the two considered geometries. When Z/R is less than the obstacle height a negative $y-$moment is apparent, which is equivalent to a pitching nose-down moment if the helicopter was facing the wall, which is consistent with the presence of the recirculation region. As the helicopter is moved upwards, the pitching moment becomes positives, as both experiments testify. This behaviour is still to be understood properly, and further investigations are in order.

5 CONCLUSIONS

In this paper a comprehensive experimental survey carried out at University of Glasgow is described, taking advantage of two different rotor rigs and several experimental techniques. Load measurements on the rotor were carried

out in order to assess the rotor performance for different rotor positions with respect to a cubic obstacle, thus simulating a set of possible hovering flights around the obstacle. Laser Doppler Anemometry (LDA) measurements of the rotor inflow were used in order to see how the aerodynamic interaction affected the rotor performance. Eventually Particle Image Velocimetry (PIV) measurements in the region between the rotor and the obstacle were carried out in order to have a better insight of the interacting flow field. The results are then compared to those previously obtained in a similar experiment carried out at Politecnico di Milano.

The investigation showed two main regions of interest. The first region is the one above the edge of the obstacle, where the thrust coefficient decreases as the rotor is positioned outwards. In this case a gradual reduction of the inflow velocity is observed going from $X/R = 1$ to $X/R = -1$, as prescribed by the ground effect. Since only part of the rotor is over the obstacle, one would expect the inflow to be non-symmetrical. However, it results to be symmetrical leading to the generation of null pitch and roll moments.

The second region, probably of more interest, is the one just beside the obstacle ($1 < X/R < 2$, $1 < Z/R < 3$), where a recirculation region between the rotor and the obstacle develops. Its morphology is deeply dependent on the rotor position. This recirculation region implies a severe thrust loss (up to 8%)with respect to the one without obstacle at the same height. This thrust loss has a maximum at approximately 2 radia from the obstacle, whereas its influence appears to be negligible when the rotor is more than 4 radia away from the obstacle. Another important feature of this region is the arising of strong pitching and rolling moments (up to 30% of the measured torque), due to the non symmetrical inflow pattern on the rotor. Limited torque variations were observed throughout the testing (less than 2%), leading to the fact that the rotor figure of merit varied mostly according to the thrust coefficient.

The comparison with a similar experiment carried out at Politecnico di Milano showed several similarities between the two experiments, thus confirming the reliability of the obtained data.

References

[1] SJ Zan. On aerodynamic modelling and simulation of the dynamic interface. *Proceedings of the Institution of Mechanical Engineers, Part G: Journal of Aerospace Engineering*, 219(5):393–410, 2005.

[2] Clement Crozon, Rene Steijl, and George N Barakos. Numerical study of helicopter rotors in a ship airwake. *Journal of Aircraft*, 51(6):1813–1832, 2014.

[3] Christopher H Kri, Yaxing Wang, Gareth D Padfield, James S Forrest, and Ieuan Owen. Aerodynamic loading characteristics of a model-scale helicopter in a ship's airwake. *Journal of Aircraft*, 49(5):1271–1278, 2012.

[4] Richard G Lee and Steven J Zan. Wind tunnel testing of a helicopter fuselage and rotor in a ship airwake. *Journal of the American Helicopter Society*, 50(4):326–337, 2005.

[5] TA Quinliven and KR Long. Rotor performance in the wake of a large structure. In *American Helicopter Society 65th Annual Forum*, May 2009.

[6] Ganesh Rajagopalan, Saeid Niazi, Alan J. Wadcock, Gloria K. Yamauchi, and Mark J. Silva. Experimental and computational study of the interaction between a tandem-rotor helicopter and a ship. In *American Helicopter Society 61st Annual Forum*, June 2005.

[7] Naohiro Iboshi, Noriaki Itoga, JVR Prasad, and Lakshmi N Sankar. Ground effect of a rotor hovering above a confined area. *Frontiers in Aerospace Engineering*, 3(1), 2014.

[8] Gisueppe Gibertini, Donato Grassi, Cesare Parolini, Daniele Zagaglia, and Alex Zanotti. Experimental investigation on

the aerodynamic interaction between a helicopter and ground obstacles. *Proceedings of the Institution of Mechanical Engineers, Part G: Journal of Aerospace Engineering*, 229(8):1395–1406, 2015.

[9] Ajay K Prasad. Stereoscopic particle image velocimetry. *Experiments in fluids*, 29(2):103–116, 2000.

[10] G. Gibertini, C. Clavel, D. Grassi, C. Parolini, D. Zagaglia, and A. Zanotti. An experimental set up for the study of helicopter and building aerodynamic interaction. Southampton, UK, September 2-5 2014. 40^{th} European Rotorcraft Forum.

Copyright Statement

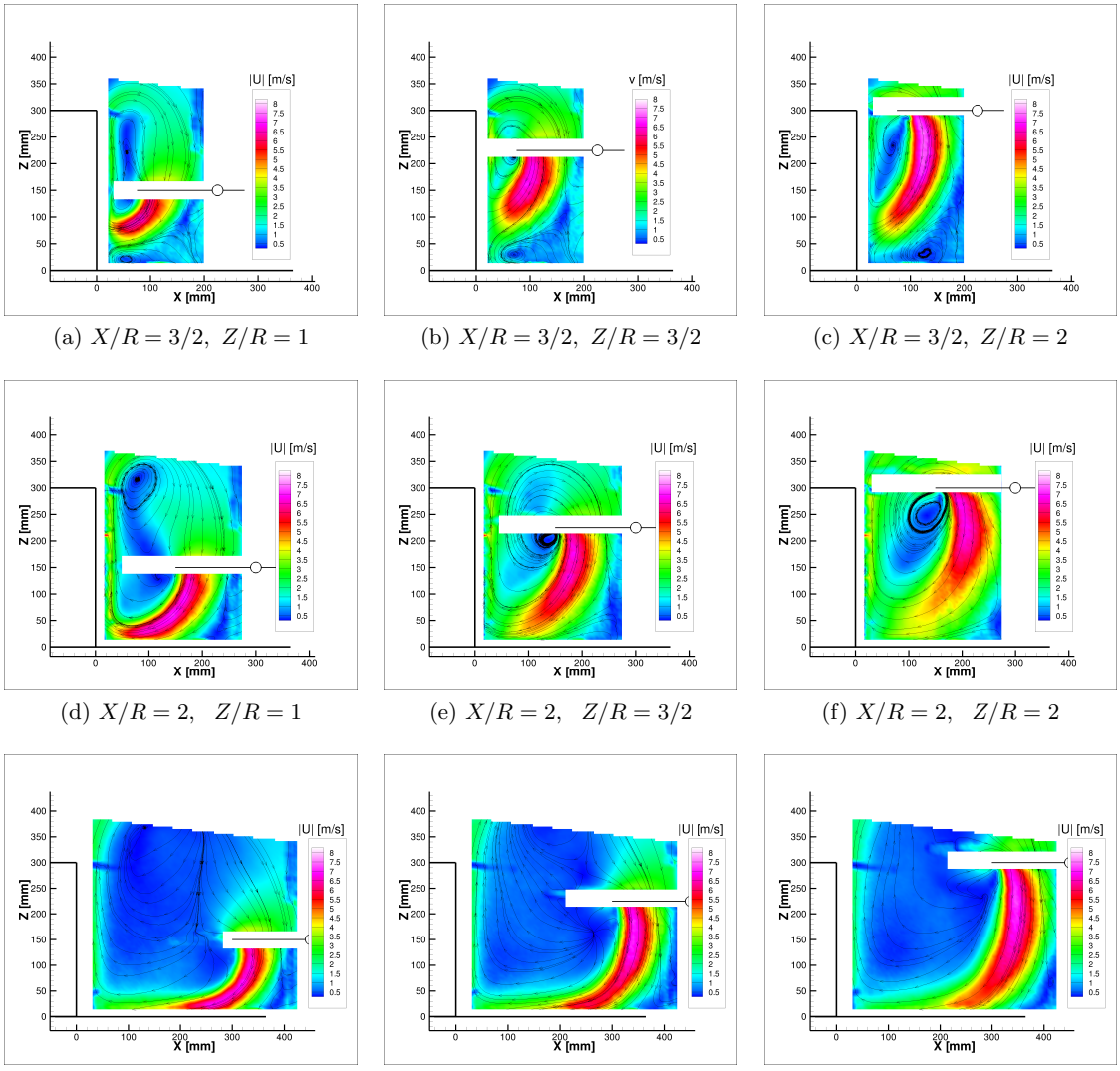

(a) $X/R = 3/2,\ Z/R = 1$ (b) $X/R = 3/2,\ Z/R = 3/2$ (c) $X/R = 3/2,\ Z/R = 2$

(d) $X/R = 2,\ \ Z/R = 1$ (e) $X/R = 2,\ \ Z/R = 3/2$ (f) $X/R = 2,\ \ Z/R = 2$

(g) $X/R = 3,\ \ Z/R = 1$ (h) $X/R = 3,\ \ Z/R = 3/2$ (i) $X/R = 3,\ \ Z/R = 2$

Figure 7: PIV Measurments. In-plane velocity magnitude contours and In-plane streamlines in the problem symmetry plane ($Y/R = 0$) for different rotor positions with respect to the obstacle